Recent Advances in Feature Scale Simulation

A. Kersch, G. Schulze Icking-Konert

Infineon Technologies AG, MP SIM
Otto-Hahn-Ring 6, D-81730 Munich, Germany; email Alfred.Kersch@infineon.com

Abstract

Recent developments for the simulation of kinetic energy driven processes on the submicron scale are presented. Examples include the deposition of ions (IPVD), reactive ion etching (RIE), and ion enhanced chemical reactions (new model for high density plasma deposition). The simulation results are discussed and are found to be in good qualitative agreement with experimental measurements.

Introduction

Feature scale simulation is likely to become a strategic tool in the development of deep submicron process technology. This is due to the extreme aspect ratios in current device technologies and the need to extend the etch and deposition processes for even faster shrink cycles. Physically based models for simulations can generate knowledge and insight which help to reduce development cycle time and cost (1).
This paper focuses on model development of directional etch and of deposition in submicron features. In addition to thermally activated surface reactions, incident energy and angular dependence of surface processes become the key quantity. Although the knowledge of the physical and chemical models is still incomplete, in some cases the combination of available information already leads to models with a predictive capability.

Basic Models

Significant effort is being made to model highly nonthermal deposition techniques using the molecular dynamics (MD) approach. Usually energy and angular dependencies of kinetic energy driven processes are calculated near threshold where experimental data is sparse. Some typical results are given in (2)-(4). The thus obtained rates as well as rates for thermally activated processes can be employed in an atomistic cellular automaton model (2), string model (1) or level set model (5) to describe the topography of the growing film.
The simulations shown here have been obtained with an in house Monte Carlo cellular automaton model CATS where particles are launched according to a calculated energy and angular distribution (from a plasma sheath model (6)), interact with the walls of the feature according to the reaction rates (reflection, sputtering, reaction), and finally deposit as a „volume cell" of a typical size of $10A \times 10A$.

Ionized physical vapor deposition (IPVD) of Ti

IPVD is used to extend the PVD technology for the fabrication of metallic barrier and seed layers to aspect ratios of 3 and more. The partially ionized, energetic particle flux not only results in an improved directionality but also affects the film properties by the energy deposition (7).
Fundamental models of such processes have a high predictive capability. We have calculated the reaction probabilities of Ti^+ and Ar^+ on Ti(200) (Fig. 1) including the energy and angular distributions of the final states (8) and have implemented them into CATS. Together with the Ar^+ , Ti^+, and Ti fluxes and distribution functions from the sheath model we obtain the film growth front including properties like stoichiometric composition, redeposition, and energy deposition. The results from Fig. 2 show the different film growth condition for trench bottom and side walls. The correlation with electrical data is suggested by the known energy deposition / film morphology relationship (9).

RIE-lag in deep trench etch

Reactive ion etching (RIE) is a kinetic energy driven process where chemical reactions occur additional to the above physical processes. In spite of their complexity some general mechanisms can be simulated. One relevant effect is the RIE-lag, the aspect dependent etch rate (10). We propose a mechanism utilizing the energy dependence of the ion assisted etch reaction. We have implemented a typical mechanism similiar to (11) into CATS parametrized by sticking coefficients S together with the energy and angular dependent yield (see Fig. 3).

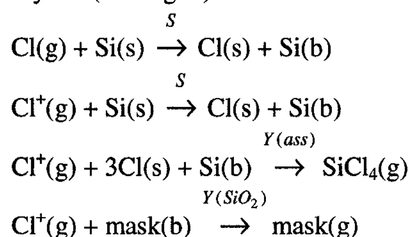

$$Cl(g) + Si(s) \xrightarrow{S} Cl(s) + Si(b)$$

$$Cl^+(g) + Si(s) \xrightarrow{S} Cl(s) + Si(b)$$

$$Cl^+(g) + 3Cl(s) + Si(b) \xrightarrow{Y(ass)} SiCl_4(g)$$

$$Cl^+(g) + mask(b) \xrightarrow{Y(SiO_2)} mask(g)$$

The reflection of neutrals is diffuse. The reflection of energetic ions with a reflection function similiar to Fig. 1 (d) (almost specular at large angles of incidence but more diffuse at smaller angles) leads to energy loss. The energy loss from reactions at the side wall increases this loss. Fig. 4 shows simulation results of a deep trench etch through a hard mask

0-7803-6441-4/00/$10.00 (C) 2000 IEEE

for two Cl^+ fluxes of equal energy but different angular distributions (3° and 6° FWHM, respectively). The results show the Rie-lag as a result of this energy loss (Fig. 5) and provide an explanation of the known correlation between the lag and the collisionality of the plasma sheath independent from the details of the chemical mechanism.

High density plasma (HDP) deposition of SiO_2

HDP deposition of SiO_2 into shallow trench isolation (STI) structures has become a mainstream isolation technique. For future generation aspect ratios will exceed 4 (12). Furthermore, extended Alu-RIE processes need intermetal dielectric deposition (IMD) processes for AR>4. Void free HDP deposition into these aspect ratios requires significant process optimizations.

In an Ar or He based high density plasma the SiH_4 and O_2 precursor are partially decomposed and ionized. The ionized species are accelerated in the plasma sheath by the electrical field which depends on the RF bias power applied to the chuck. The energetic ions cause ion assisted deposition as well as sputter etch.

We have developed a fundamental model for the HDP deposition of SiO_2 where the energy dependence of the processes plays a major role. Using AURORA (13) we have analyzed the chemical mechanisms in the plasma and on the surface as proposed by (14). The reaction rates in this model have been calibrated to planar deposition. For ion fluxes in the normal direction the deposition rate limiting step turns out to be oxygen incorporation whereas for much lower ion fluxes – e.g. at feature side walls – the rate limiting step is the ion assisted surface reconstruction from the inert $SiG(OH)H_2$ to the reactive SiG_3H surface state. Only after this reconstruction the deposition can proceed chemically (Fig. 6). An exception are hyperthermal, neutral sputter products which deposit directly. The information needed to extend the planar to the non-planar deposition model inside a feature is the energy and angular dependent yield of the surface activation $Y_{act}(E,\theta)$. Additionally knowledge of the energy and angular dependence of the sputter etch yield $Y_{SiO2}(E,\theta)$ is required. We have also used AURORA to reduce the surface model to an effective model with O(g) and SiO(g) as oxygen and silicon containing reactive radicals, H(g) as hydrogen, $Ar^+(g)$ as the only sigificant ion, $O^*(s)$ and $SiO^*(s)$ as passivated and O(s) and SiO(s) as activated surface sites and SiO(b) and O(b) bulk material. The effective sticking coefficients are obtained from the reduction of the Meeks model. Ref. (4) gives MD results for $Y_{SiO2}(E,\theta)$ including the energy and angular distribution of sputtered and reflected particles (Fig. 3). $Y_{act}(E,\theta)$ is unknown and reasonable values had to be assumed. We have choosen the energy dependence as a saturating function with low threshold in accordance with measurements and have guessed the angular dependence to reproduce the observed shape. Our complete model is (X = O or SiO and $\underline{X}$ if hyperthermal):

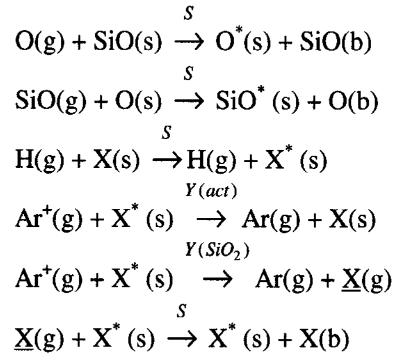

$$O(g) + SiO(s) \xrightarrow{s} O^*(s) + SiO(b)$$
$$SiO(g) + O(s) \xrightarrow{s} SiO^*(s) + O(b)$$
$$H(g) + X(s) \xrightarrow{s} H(g) + X^*(s)$$
$$Ar^+(g) + X^*(s) \xrightarrow{Y(act)} Ar(g) + X(s)$$
$$Ar^+(g) + X^*(s) \xrightarrow{Y(SiO_2)} Ar(g) + \underline{X}(g)$$
$$\underline{X}(g) + X^*(s) \xrightarrow{s} X^*(s) + X(b)$$

Figures 7 and 8 show the main phenomena filling a test structure. At low bias power the growth is anisotropic with a small side wall growth caused by reflected ions and thermal activation. At high bias power sputter etch is activated which leads to corner beveling and increased side wall growth due to redeposition of sputtered material. The anisotropic growth allows the deposition into test structures like in Figures 9-11. Visible in Fig. 9 (a) is the typical onion shaped dome at low bias power. In DRAM applications, however, material densification is required for reliability reasons. This can be achieved by higher bias power deposition. But then the redeposition may prohibit a successful fill as is shown in Figure 9 (b). Visible is also the flat beveling angle at the top typical for higher bias power deposition. Using the calibrated model process optimization with respect to flow rate, pressure, and bias power has been supported.

References

(1) T.S.Cale, T.P.Merchant, L.J.Borucki and A.H.Labun, "Topography simulation for the virtual wafer fab", Thin Solid Films **365**, 152 (2000)

(2) U.Hansen, P.Vogl and V.Fiorentini, „Atomistic modeling of large-scale metal film growth fronts", Phys.Rev. B **59**, 7856 (1999)

(3) U.Hansen and A.Kersch, „Reaction rates for ionized physical vapor deposition modeling from molecular dynamics calculations: The effect of surface roughness", Phys.Rev. B **60**, 14417 (1999)

(4) C.Abrams, D.Graves, „Energetic ion bombardement of SiO_2 surfaces: Molecular dynamics simulations", J.Vac.Sci.Technol. A **16**, 3006 (1998)

(5) U.Hansen, S.Rodgers and K.F.Jensen, „Modeling of metal thin film growth: Linking angstrom-scale molecular dynamics results to micron-scale film topographies", Phys.Rev. B **62**, 2869 (2000)

(6) M.Kratzer, R.P.Brinkmann, H.Schmidt, „A hybrid model for the calculation of ion distribution functions behind a DC or RF driven plasma boundary sheath", unpublished

(7) D.C.Butler, K.Buchanan, S.R.Burgess, N.Urbansky and S.Schmidbauer, Solid State technology, July 2000

(8) A.Kersch and U.Hansen, „An atomistic and feature scale model for the ionized physical vapour deposition of Titanium", unpublished

(9) J.A.Thornton, J.Vac.Sci.Technol. **11**, 666 (1974)

(10) K.P.Müller, K.Roithner and H.-J. Timme, „Selectivity and Si-load in deep trench etching", Microelectronic Engineering **27**, 457 (1995)

(11) J.P.Chang, H.H.Sawin, J.Vac.Sci.Technol. A **16**, 217 (1998)

(12) L.Peters, Semiconductor International, Vol **23**, March 2000

(13) AURORA, Reaction Design, www.ReactionDesign.com

(14) E.Meeks, R.S.Larson, P.Ho, S.M.Han, E.Edelberg, E.Aydil, C.Apblett, „Modeling of SiO_2 deposition in high density plasma reactors and comparisons of model predictions with experimental measurements", J.Vac.Sci.Technol. A**16**, 544 (1998)

0-7803-6441-4/00/$10.00 (C) 2000 IEEE

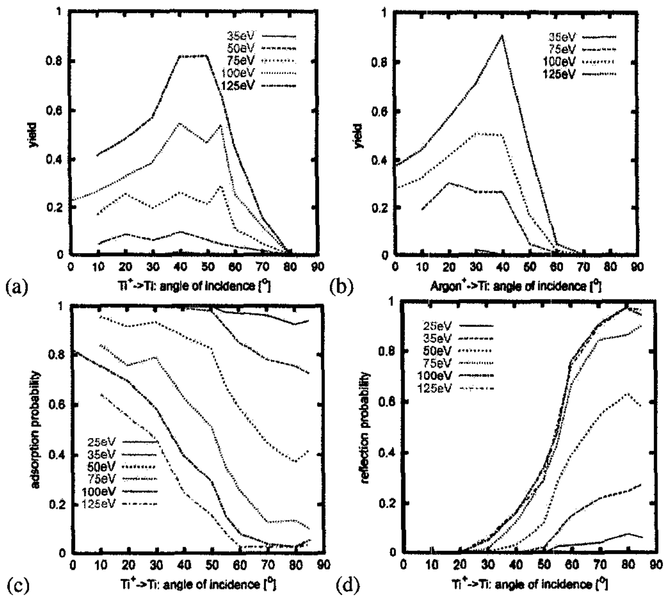

Fig. 1: Yield of $Ti^+ \rightarrow Ti(002)$ (a) and $Ar^+ \rightarrow Ti(002)$ (b) as a function of incident angle and energy. Adsorption (c) and reflection probability (d) of $Ti^+ \rightarrow Ti(002)$.

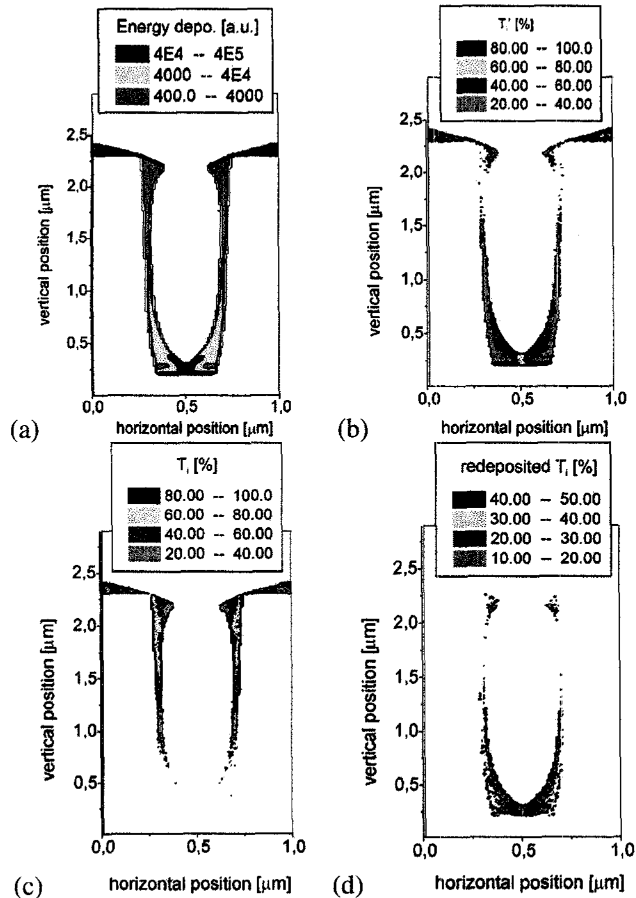

Fig. 2: Relative species fluxes: $f(Ar^+)/f(Ti)=10$, $f(Ti^+)/f(Ti+Ti^+)=0.7$, 120V RF bias. Results: (a) total energy deposition from ions, (b) deposited ions, (c) deposited neutrals, (d) redeposited material.

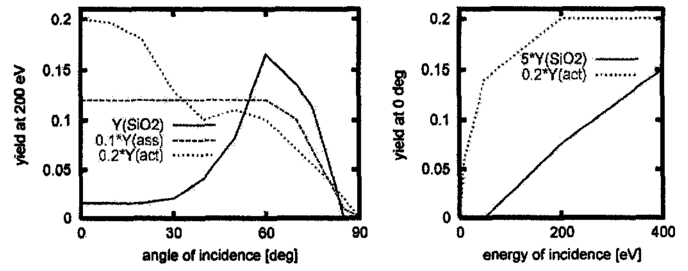

Fig. 3: Yield functions used: $Y(SiO_2)$ taken from MD [4]. Y(ass) is calibrated to avoid sidewall bowing in the absence of a passivation mechanism. Y(act) is estimated.

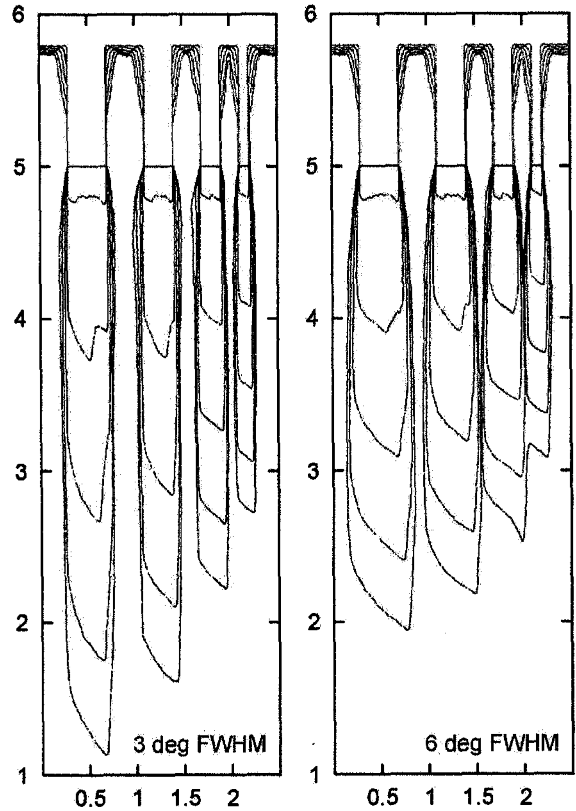

Fig. 4: CATS simulation of deep trench etch through a hard mask with model [11]. The angular distributions of 3° and 6° FWHM correspond to plasma sheaths with different collisionality.

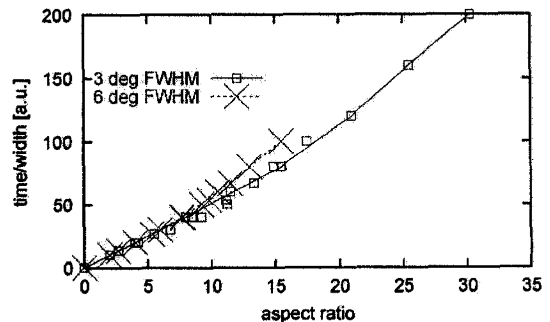

Fig. 5: Etch time to reach respective aspect ratio as obtained from Fig. 4. Here "width" refers to the opening of the mask. The nonlinearity is the RIE-lag.

0-7803-6441-4/00/$10.00 (C) 2000 IEEE

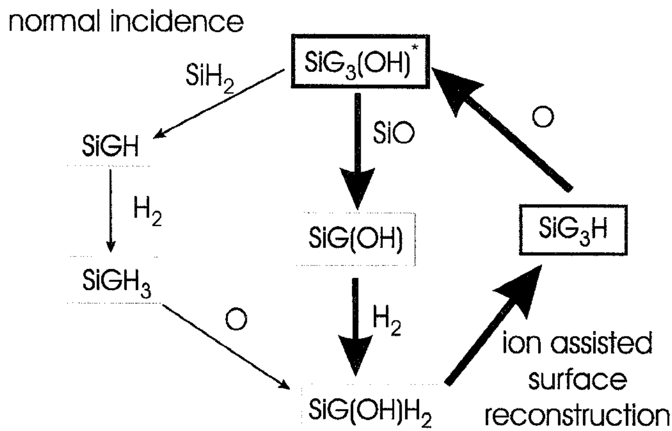

Fig. 6: Relevant reaction paths from (14) for normal incidence of Ar^+. The thickness of boxes and arrows indicate the respective coverage and conversion rates. For normal ion flux the rate limiting step is O incorporation whereas for glancing ion angles it is the ion assisted surface reconstruction. In the CATS model the passivated state $SiG(OH)H_2$ is represented by O^* or SiO^* and the activated state SiG_3H by O or SiO, respectively.

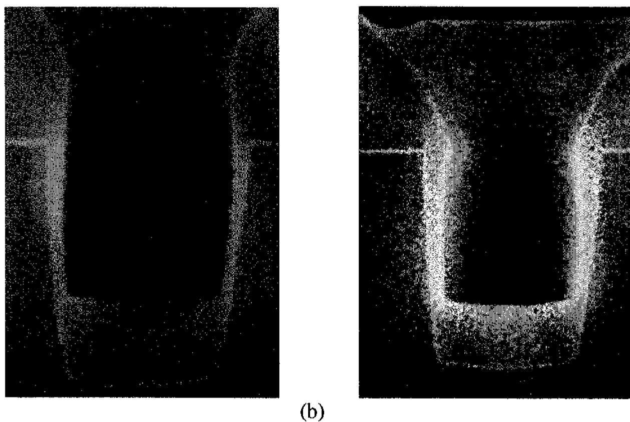

(a) (b)

Fig. 7: SiO_2 deposition from Ar based HDP under standard conditions (a) with low bias power and (b) with high bias power into a test structure.

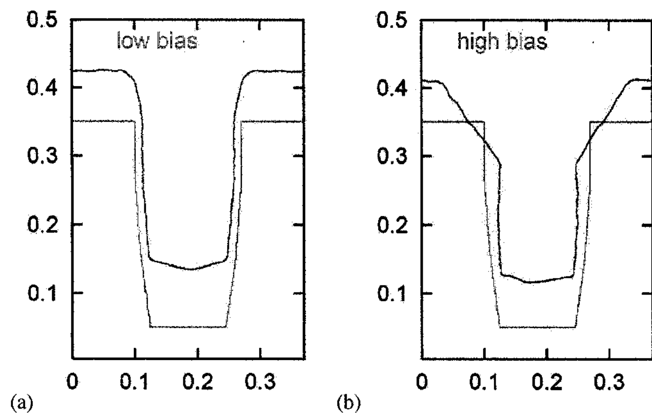

(a) (b)

Fig. 8: CATS simulation results corresponding to Fig. 7 (a) and (b).

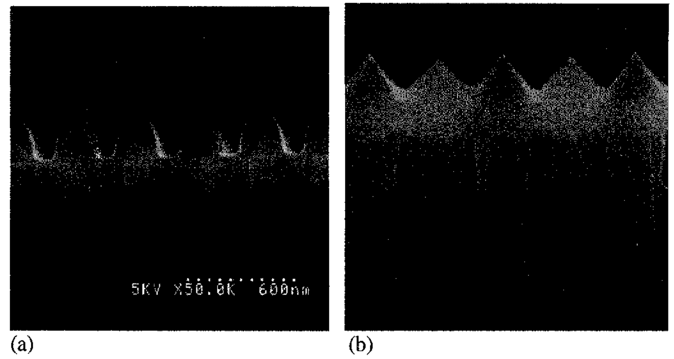

(a) (b)

Fig. 9: SiO_2 deposition from HDP under standard conditions (a) with low bias power into AR=3 and (b) with high bias power into AR=4 test structure.

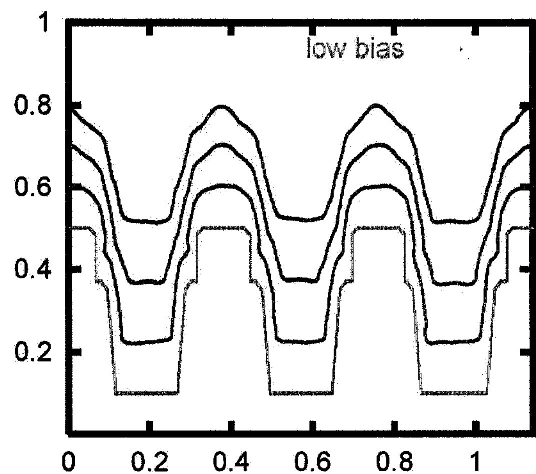

Fig. 10: CATS simulation result for deposition into structure 9 (a). The anisotropic growth at low bias power produces a characteristic onion shaped dome and a completely filled structure.

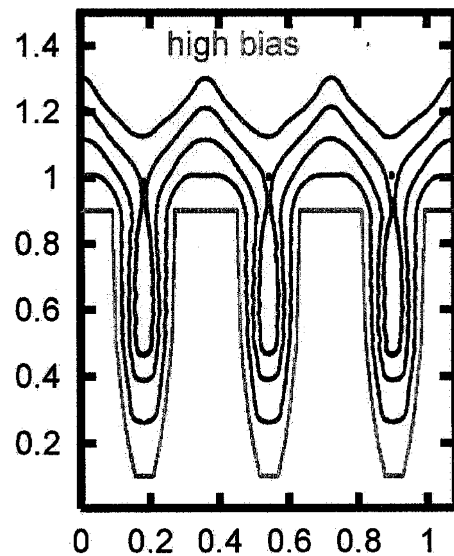

Fig 11: CATS simulation result for deposition into structure 9 (b). The redeposition at higher bias power prevents the structure to be completely filled. Characteristic is the flat beveling angle.

0-7803-6441-4/00/$10.00 (C) 2000 IEEE